Localized diabatization applied to excitons in molecular crystals

Zuxin Jin and Joseph E. Subotnik

Citation: The Journal of Chemical Physics **146**, 244110 (2017); doi: 10.1063/1.4986952
View online: http://dx.doi.org/10.1063/1.4986952
View Table of Contents: http://aip.scitation.org/toc/jcp/146/24
Published by the American Institute of Physics

Localized diabatization applied to excitons in molecular crystals

Zuxin Jin[1] and Joseph E. Subotnik[1,2]
[1]*Department of Chemistry, University of Pennsylvania, Philadelphia, Pennsylvania 19104, USA*
[2]*Stanford PULSE Institute, SLAC National Accelerator Laboratory, Menlo Park, California 94025, USA*

(Received 6 February 2017; accepted 7 June 2017; published online 28 June 2017)

Traditional *ab initio* electronic structure calculations of periodic systems yield delocalized eigenstates that should be understood as adiabatic states. For example, excitons are bands of extended states which superimpose localized excitations on every lattice site. However, in general, in order to study the effects of nuclear motion on exciton transport, it is standard to work with a localized description of excitons, especially in a hopping regime; even in a band regime, a localized description can be helpful. To extract localized excitons from a band requires essentially a diabatization procedure. In this paper, three distinct methods are proposed for such localized diabatization: (i) a simple projection method, (ii) a more general Pipek-Mezey localization scheme, and (iii) a variant of Boys diabatization. Approaches (i) and (ii) require localized, single-particle Wannier orbitals, while approach (iii) has no such dependence. These methods should be very useful for studying energy transfer through solids with *ab initio* calculations. *Published by AIP Publishing.* [http://dx.doi.org/10.1063/1.4986952]

I. INTRODUCTION

Excitons are electrically neutral quasiparticles which can be viewed as bound electron-hole ($e-h$) pairs and are closely associated with a wide range of transport phenomena and optical properties. Understanding excitons and excitonic energy transfer is a hot topic in modern materials chemistry[1] with both practical implications for devices and theoretical implications for condensed matter theory as the interactions of excitons with phonons yield another quasiparticle, the polaron.[2]

To study excitons in periodic solids with *ab initio* methods, the standard approach is to solve the Bethe-Salpeter equation (BSE),[3–10] though time-dependent density functional theory (TDDFT)[11–14] is an alternative method. Within the context of TDDFT, several exchange-correlation functionals have been proposed or studied for excitons.[15–17] A general review can be found in Ref. 18. Within both the BSE and TDDFT approaches, the charge density of excited states preserves the underlying lattice translational symmetry. In other words, even in the tight-binding limit, BSE and TDDFT eigenstates are superpositions of individual excitons, and these superpositions form excitonic bands: an individual electron-hole pair is never completely isolated. To probe the localized nature of electrons and holes, one can define a correlation function $\mathcal{F}(\boldsymbol{r})$ that describes the probability of finding the electron and hole separated by $\boldsymbol{r}$.[10]

Unfortunately, despite the convenience of using periodic wave functions to describe excited states in extended systems, there are several models of energy transfer in periodic systems that work naturally with a localized picture of excited states, most famously the Holstein model.[19,20] In particular, nuclear motion can drive localization of excitons, such that hopping becomes the dominant mechanism of energy transfer; in the extreme tight-binding limit, one can calculate energy transfer rates between neighboring unit cells with Marcus theory.[21] In such a case, with strongly coupled nuclear motion, truly localized excitonic states (or polarons) are long-lived, and we require models of such meta-stable states to model nuclear-electronic dynamics easily.

The scenario above is not new in the context of quantum chemistry. There is an enormous literature in molecular chemistry discussing the proper framework for switching between adiabatic and diabatic representations, going back several decades.[22–27] If the total Hamiltonian is $H = T_n + H_e$, where T_n is the nuclear kinetic energy and H_e is the electronic Hamiltonian, the adiabatic representation relies on diagonalizing the electronic Hamiltonian (H_e) and the resulting electronic adiabatic states can change dramatically with nuclear position; by contrast, the diabatic representation attempts to keep the same physical character for each electronic state for all nuclear positions.[28–32] Very often, diabatic states localize the charge or excitation character of a given electronic state.[33–42]

Today, there are a plethora of approaches for generating adiabatic-to-diabatic transformations (ADT) for molecular systems, sometimes based on a physical observable[33] and sometimes based on projecting out various target configurations.[43,44] There are also alternative approaches for constructing diabatic states directly, including constrained DFT (C-DFT)[45] and frozen-density functional theory.[46–49] In all of the approaches above, the diabatic states are many-electron states which are built up by accounting for as much electron-electron correlation as possible while keeping the character of the electronic states immutable with nuclear geometry.

Now, obviously, many-electron states are not orbitals, but there are clear connections between many-electron state diabatization and single orbital localization protocols.[40,41] For example, in quantum chemistry, Boys localization can be applied both to the localization of single particle orbitals[50] and the diabatization of many-electron states.[40] For the reader who is unaccustomed to the distinction above, a brief review is now in order.

A. Boys localization of single particle orbitals

First, consider the localization of orbitals. If we begin with a set of M single-particle molecular orbitals, $\{|\phi_j\rangle, j = 1, 2, \ldots, M\}$, Boys localization produces localized single-particle orbitals $\{|\eta_j\rangle, j = 1, 2, \ldots, M\}$ through rotation,

$$|\eta_j\rangle = \sum_i |\phi_i\rangle U_{ij}. \tag{1}$$

The U matrix prescribed above is defined by separating charge centers as far away from each other as possible. In other words, according to Boys localization, one maximizes

$$f^{sp}_{Boys}(U) = \sum_{i,j=1}^{M} (\langle\eta_i|\boldsymbol{r}|\eta_i\rangle - \langle\eta_j|\boldsymbol{r}|\eta_j\rangle)^2. \tag{2}$$

Because the trace is invariant with respect to a unitary transform, Boys localization is equivalent[51] to maximizing

$$f^{sp}_{Boys}(U) = \sum_{j=1}^{M} (\langle\eta_j|\boldsymbol{r}|\eta_j\rangle)^2 \tag{3}$$

or minimizing the quadratic spread,

$$f^{sp}_{Boys}(U) = \sum_{j=1}^{M} \left(\langle\eta_j|r^2|\eta_j\rangle - (\langle\eta_j|\boldsymbol{r}|\eta_j\rangle)^2\right). \tag{4}$$

B. Maximally localized Wannier functions

Second, for the reader with a chemistry (as opposed to solid-state) background, note that maximally localized Wannier functions (MLWFs)[52] are equivalent to Boys localization applied to a periodic solid. In this case, if we begin with a set of M single-particle Bloch bands $\{|\phi_i^{(\boldsymbol{k})}\rangle, i = 1, 2, \ldots, M\}$ which are isolated from all other bands, MLWFs are localized single-particle orbitals $\{|\eta_j^{(\nu)}\rangle, j = 1, 2, \ldots, M\}$ through "rotation,"

$$|\eta_j^{(\nu)}\rangle = \frac{V_{cell}}{(2\pi)^3} \int_{\text{B.Z.}} \mathrm{d}\boldsymbol{k} e^{-i\boldsymbol{k}\cdot\boldsymbol{R}_\nu} \sum_i |\phi_i^{(\boldsymbol{k})}\rangle U_{ij}^{(\boldsymbol{k})}. \tag{5}$$

Here, the band is indexed by i and j, the crystal momentum of the Bloch states is indexed by $\boldsymbol{k}$, and the unit cell of the Wannier function (WF) is labeled by ν. If we apply periodic boundary condition (PBC) over a finite number of unit cells, the integral over $\boldsymbol{k}$ will become a sum. The U matrix prescribed above is defined by minimizing the single-particle quadratic spread function in the home unit cell (denoted by $\mathbf{0}$) $f^{sp}_{MLWF}(U)$

$$f^{sp}_{MLWF}(U) = \sum_j \left[\langle\eta_j^{(\mathbf{0})}|r^2|\eta_j^{(\mathbf{0})}\rangle - (\langle\eta_j^{(\mathbf{0})}|\boldsymbol{r}|\eta_j^{(\mathbf{0})}\rangle)^2\right]. \tag{6}$$

Matrix elements of the position operator between WFs are usually evaluated in reciprocal space.[53] Every WF constructed by Eq. (5) at one site $\boldsymbol{R}_\nu$ will have translational images at all other sites $\boldsymbol{R}_{\nu'}$. Thus, to define the criterion function f, it suffices to minimize the spread of all Wannier functions labeled by a single unit cell [usually the origin, as in Eq. (6)].

Now, for our purposes below, it will be helpful to construct MLWFs through an alternative, one-step procedure [without applying a Fourier transform explicitly, as in Eq. (5)].

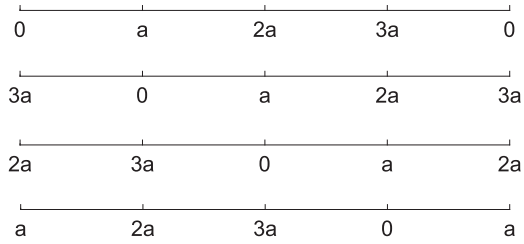

FIG. 1. A schematic diagram of the cyclically permuted position operators. Periodic boundary conditions (PBCs) are applied over 4 unit cells.

In particular, it will be helpful to find a simple extension of the Boys localization function in Eq. (3) as relevant for the solid state. Note that this extension must take into account all unit cells with equal weight so that the resulting localized Wannier orbitals are localized equivalently to every lattice site.

With this in mind, the relevant extension of Boys localization function is straightforward. Without loss of generality, consider a 1D crystal with lattice constant a and suppose that we enforce periodic boundary conditions over N unit cells. Thus, our entire region of interest is the domain $[0, Na)$. Let $X^{(0)}$ be the position operator on $[0, Na)$. We will then define a set of $N-1$ cyclically permuted operators $X^{(d)}$, $d = 1, \ldots, N-1$, with the d-th operator mapping the domain $[0, Na)$ onto $[(N-d)a, Na) \cup [0, (N-d)a)$. See Fig. 1. These cyclically permuted position operators are smooth except for a single discontinuity when the position resets to zero. Finally, a set of well-localized WFs can be constructed through maximizing

$$f^{sp}_{Boys-periodic}(U) = \sum_{j,\nu} \sum_{d=0}^{N-1} \langle\eta_j^\nu|X^{(d)}|\eta_j^\nu\rangle^2, \tag{7}$$

where $|\eta_j^\nu\rangle = \sum_{ik} |\phi_i^{(\boldsymbol{k})}\rangle U_{i\boldsymbol{k},j\nu}$ is a (hopefully localized) single-particle state to be determined.

Equation (7) is entirely analogous to Eq. (6); the square term $\sum_{j\nu d} \langle\eta_j^\nu|(X^{(d)})^2|\eta_j^{(\nu)}\rangle$ has been dropped due to the invariance of the trace operator. However, unlike Eq. (6)—which assumes an infinite solid without imposed wavefunction periodicity—Eq. (7) localizes Wannier functions that are explicitly defined with periodic boundary conditions. That being said, consider the WF localized around position $\boldsymbol{R}_\nu$, $|\eta_j^\nu\rangle$. Note that, as the number N goes to infinity, only an infinitesimal fraction of the operators $X^{(d)}$ will be discontinuous somewhere within the support $|\eta_j^\nu\rangle$ (i.e., where $\eta_j^\nu(\boldsymbol{r})$ is significantly nonzero). Thus, in the limit of large N, maximizing Eq. (7) becomes equivalent to minimizing the quadratic spread and generating MLWFs, as we wanted to show. Note that this approach of cyclically permuted operators can easily be extended to two and three dimensional solids and other physical quantities with lattice symmetry and periodic boundary conditions.

C. Boys localized diabatization

Third and lastly, let us consider localized diabatization within molecules. Given M many-electron adiabatic states $\{|\Psi_J\rangle, J = 1, 2, \ldots, M\}$, we may construct a quasi-diabatic

representation $\{|\Xi_L\rangle, L = 1, 2, \ldots, M\}$ by constructing a unitary transform matrix U,

$$|\Xi_L\rangle = \sum_J |\Psi_J\rangle U_{JL}. \tag{8}$$

Boys localized diabatization[41] constructs U by separating charge centers as far away from each other as possible. In other words, Boys diabatization maximizes the following function:

$$f^{diab}_{Boys}(U) = \sum_{L,L'=1}^{M} (\langle \Xi_L|\boldsymbol{r}|\Xi_L\rangle - \langle \Xi_{L'}|\boldsymbol{r}|\Xi_{L'}\rangle)^2. \tag{9}$$

Thus, Boys localized diabatization is completely analogous to Boys single-particle orbital localization. In general, Eq. (9) can be very effective for treating charge transfer and is a natural generalization of the famous Generalized Mulliken–Hush (GMH) formalism.[33]

More generally, if we wish to study energy transfer, there are two straightforward means of extending Boys localization. On the one hand, one could substitute Boys for Edmiston-Ruedenberg localized diabatization.[54] On the other hand, for CIS or TD-DFT/TDA wavefunctions, one can simply use the BoysOV variant of localized diabatization.[55]

To understand BoysOV localized diabatization, consider an excited state CIS wavefunction $|\Xi\rangle = \sum_{ia} t_{ia}|\Phi^a_i\rangle$, where i and a label occupied and virtual single-particle orbitals, respectively. For such an excited state, it is straightforward to construct the density of an effective particle (attachment) and hole (detachment) for an excited wavefunction,[56]

$$\begin{aligned} \rho_{att}(x) &= \sum_{iab} t^*_{ia} t_{ib} \phi^*_a(x)\phi_b(x), \\ \rho_{det}(x) &= -\sum_{ija} t^*_{ia} t_{ja} \phi^*_j(x)\phi_i(x). \end{aligned} \tag{10}$$

Now, according to BoysOV localized diabatization, we generated diabatic states $\{|\Xi_I\rangle\}$ by maximizing the following function to separate particle from particle and hole from hole:

$$\begin{aligned} s^{(I)}_{ia} &= \sum_J t^{(J)}_{ia} U_{JI}, \\ f^{diab}_{BoysOV}(U) &= \sum_I \left(\sum_{iab} (s^{(I)}_{ia})^* \langle \phi_a|X|\phi_b\rangle s^{(I)}_{ib} \right)^2 \\ &\quad + \sum_I \left(\sum_{ija} (s^{(I)}_{ia})^* \langle \phi_j|X|\phi_i\rangle s^{(I)}_{ja} \right)^2. \end{aligned} \tag{11}$$

Equation (11) is a very powerful generalization of Boys localized diabatization and has been previously used successfully to model energy transfer in donor-bridge-acceptor molecules.[55]

D. Our goal

Our goal is now clear. Just as Boys localization of single particle orbitals has been extended to MLWFs in periodic solids, we would like to generalize existing techniques for localized diabatization of many-electron molecular states into the realm of periodic solids; in particular, what is the generalization of Boys localized diabatization in a solid? Using Marcus theory, for example, these localized diabatic states will allow us to study energy transfer in solid-state systems.

In order to accomplish this goal, we will present three different methods below. The first method is the least general for it relies on target single-particle excitation target functions (usually chosen to be localized Wannier excitations), which may or may not be accurate. The second method is more general and can be considered a generalization of Pipek-Mezey single-particle orbitals (which were recently extended to periodic solids).[57] Like method #1, this method also relies on the existence of well-localized single-particle WFs. Finally, for the third method, we also present the generalization of Boys localized diabatization to the case of excitons in a periodic solid.

This paper is organized as follows. In Sec. II we review the basic procedure for obtaining exciton bands and provide all theoretical details. In Sec. III we apply our methods to a 1D model system. In Sec. IV we investigate and discuss the results. We conclude in Sec. V.

Regarding the notation for the rest of the paper, $\tilde{i}, \tilde{j}$ are used to represent occupied spin orbitals and $\tilde{a}, \tilde{b}$ for virtual spin orbitals. i and a label spatial occupied and virtual bands, respectively. A band index, a crystal wave vector (k or q), and spin σ all together determine a spin orbital, i.e., $\tilde{i} = (i, k, \sigma)$. In a Wannier representation, we use μ and ν to label the lattice sites where the WFs are localized. Many-electron states of a molecule are indexed with capital Roman letters $(I, B, L, \cdots)$; many-electron states of a solid (i.e., excitonic bands) are indexed with capital Roman letters (for band) and a crystal wave-vector (k or q). CIS expansion coefficients are denoted as t_{ia} (adiabatic) or s_{ia} (diabatic).

II. THEORY

A. Model

Let us neglect any deformations or vibrations of the crystal and focus exclusively on electrons in a periodic potential. For the present paper, the effect of the positive ions and core electrons is modeled by a background potential shown in Fig. 2. Our sample calculation assumes 4 electrons per unit cell, where we expect a restricted closed shell for the ground state. Let N be the number of unit cells in the solid (with periodic boundary conditions). The dependence of our results on N will be examined.

To avoid divergences of the Coulomb force in one dimension,[58] we introduce a quasi-1D phenomenological form of the effective $e - e$ interaction,[59]

$$V_{ee}(x, x') = \frac{\lambda}{\sqrt{(x - x')^2 + l^2}}, \tag{12}$$

where $1/\lambda$ is the dielectric constant of the background and l is a length parameter associated with the radius of the cylindrical wire in its original 3D problem.[59] The Fourier transform is then

$$V_{ee}(q) = 2\lambda K_0(|q|l). \tag{13}$$

Here, K_0 is the zeroth modified Bessel function of the second kind which behaves $\sim\log(1/q)$ as q approaches zero.[60]

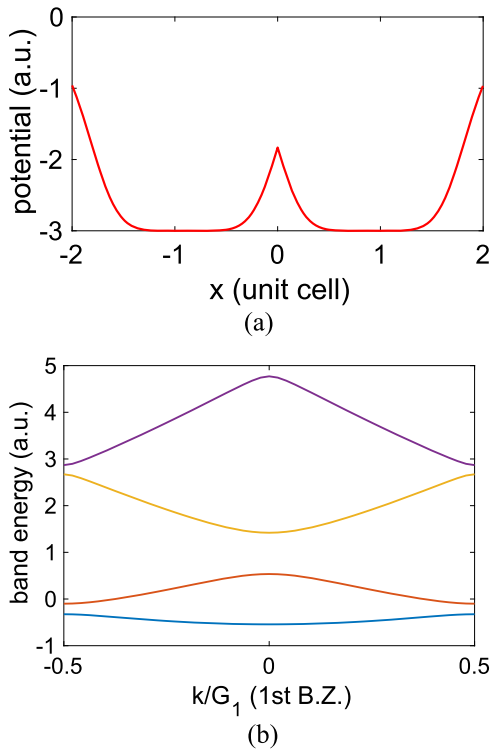

FIG. 2. (a) Lattice potential in one unit cell and (b) Hartree-Fock (single-particle) orbital band structure. The parameter l in the $e-e$ interaction [Eq. (12)] is chosen to be 2 throughout this paper. $\lambda = 1$ in this figure.

For the present paper, we solve for the ground state of the solid using a simple HF ansatz.

B. Identifying the excitons

The excited states of a solid must preserve translational symmetry and thus can be labeled by a quantum number q. To the lowest order approximation, we will construct excited states $|\Psi_q\rangle$, with single excitations $|\Phi_i^a\rangle$,

$$|\Psi_q\rangle \equiv \sum_{i,a,k,\sigma} t_{i,k,\sigma}^{a,k+q,\sigma} |\Phi_{i,k,\sigma}^{a,k+q,\sigma}\rangle. \tag{14}$$

The excitation energies and coefficients t are determined by the configuration interaction singles (CIS) eigenvalue equations,

$$\boldsymbol{At} = \boldsymbol{Et} \tag{15}$$

with

$$A_{\tilde{i}\tilde{a},\tilde{j}\tilde{b}} = (\epsilon_{\tilde{a}} - \epsilon_{\tilde{i}})\delta_{\tilde{i}\tilde{j}}\delta_{\tilde{a}\tilde{b}} + \langle \tilde{a}\tilde{j}||\tilde{i}\tilde{b}\rangle, \tag{16}$$

where ϵ is the energy of a HF orbital and δ is a Kronecker delta function.

Note that, for CIS states, S_z is conserved, and thus the spin of occupied orbital i (σ_i) must match the spin of virtual orbital a (σ_a). For singlets, we require $t_{i,k,\uparrow}^{a,k',\uparrow} = t_{i,k,\downarrow}^{a,k',\downarrow}$, and for triplets we require $t_{i,k,\uparrow}^{a,k',\uparrow} = -t_{i,k,\downarrow}^{a,k',\downarrow}$. For realistic calculations on experimental systems, $\langle \tilde{a}\tilde{j}||\tilde{i}\tilde{b}\rangle$ can be replaced by $\langle \tilde{a}\tilde{j}|(1+w)|\tilde{i}\tilde{b}\rangle$ with w an appropriate density functional; this formalism converts CIS into TDDFT with the Tamm-Dancoff approximation.[61] For any excited state calculation in a solid, the conduction and valence bands should be included at minimum.

Let us now move to the Wannier picture. Note that every periodic wave function can be expanded in a local basis, so that

$$|\Phi_{i,k}^{a,k+q}\rangle = \frac{1}{N}\sum_{\mu\nu} e^{i[(k+q)R_\mu - kR_\nu]} |\Phi_{i,\nu}^{a,\mu}\rangle. \tag{17}$$

Of course, a general wave function $|\Psi_q\rangle$ [as in Eq. (14)] generally has components $|\Phi_{i,\nu}^{a,\mu}\rangle$ with $\mu \neq \nu$. That being said, there will be bands of states (hereafter, labeled $|\xi_q^{(n)}\rangle$ and indexed by n) which are mainly superpositions of localized Wannier excitations $|\Phi_{i,\nu}^{a,\nu}\rangle$ and for which we expect

$$|\xi_q^{(n)}\rangle \sim \sum_{i,a,\nu} C_{ia}^{(n)} e^{iqR_\nu} \left(|\Phi_{i,\nu,\uparrow}^{a,\nu,\uparrow}\rangle \pm |\Phi_{i,\nu,\downarrow}^{a,\nu,\downarrow}\rangle\right) + \text{small terms} \tag{18}$$

for some coefficients $C_{ia}^{(n)}$.

Before diabatizing an excitonic band, we would like to confirm the nature of such a putative exciton band. Obviously, for many semiconductors and organics, we find excitonic bands in the band gap, but an explicit test for the excitonic character will be helpful for our model study. To identify $|\xi_q^{(n)}\rangle$ as an excitonic band, one can certainly use a scaling approach[62] that adjusts the parameter λ in Eq. (12) (which plays the role of inverse dielectric constant). Thereafter, one can monitor how the excitation energies change with varying λ. Excitonic states should not be sensitive to such scaling and behave differently from simple particle-hole excitations. An alternative, cheaper method for identifying excitons near the Frenkel limit is to calculate a localization criterion,

$$f(|\Psi_q\rangle) = \sum_{i,a,\nu,\sigma} |\langle \Phi_{i,\nu,\sigma}^{a,\nu,\sigma}|\Psi_q\rangle|^2 = \frac{2}{N}\sum_{i,a}\left|\sum_k t_{i,k,\uparrow}^{a,k+q,\uparrow}\right|^2 \tag{19}$$

for each excited state. By definition, for $|\xi_q\rangle$ defined in Eq. (18), $f(|\xi_q\rangle)$ will be much larger than $f(|\Psi_q\rangle)$ for all other $|\Psi_q\rangle$; in the tight-binding (TB) limit $f_{TB}(|\xi_q\rangle) \sim 1$.

C. Diabatization

We are now in a position to extract localized diabatic states $\{|\Xi\rangle\}$ from extended adiabatic excitonic states. In many cases, only the lowest exciton band ($\{|\xi_q\rangle\}$) is energetically favored (so we can neglect the excitonic band index I),

$$|\Xi_\mu\rangle = \sum_q |\xi_q\rangle e^{i\boldsymbol{q}\cdot\boldsymbol{R}_\mu} e^{i\theta(\boldsymbol{q})} \equiv \sum_q |\xi_q\rangle U_{q\mu}. \tag{20}$$

More generally, diabatization can disentangle two or more excitonic bands [see Eq. (5)],

$$|\Xi_\mu^B\rangle = \sum_q e^{i\boldsymbol{q}\cdot\boldsymbol{R}_\mu} \sum_I |\xi_q^I\rangle \tilde{U}_{IB}^{(q)} \equiv \sum_{Iq} |\xi_q^I\rangle U_{Iq,B\mu}. \tag{21}$$

1. Method #1

Our first many-electron diabatization scheme is a variation of the simple projection method that is used to construct one-particle WFs.[63] The basic idea of method #1 is to find a smooth gauge for the Bloch states by projecting them onto target functions[43] that roughly resembles localized excitons, e.g., localized Wannier excitations. Suppose we have M

excitonic bands to diabatize. First we choose a set of M localized target functions $\{|g_J\rangle, J = 1, \ldots, M\}$, and project them onto the exciton manifold,

$$|\zeta_{\boldsymbol{q}}^J\rangle = \sum_I |\xi_{\boldsymbol{q}}^I\rangle\langle\xi_{\boldsymbol{q}}^I|g_J\rangle. \tag{22}$$

The set $\{|\zeta_{\boldsymbol{q}}^J\rangle\}$ is typically smooth in $\boldsymbol{q}$, but not orthonormal. Next, denote the overlap matrix $(S_{\boldsymbol{q}})_{JJ'} = \langle\zeta_{\boldsymbol{q}}^J|\zeta_{\boldsymbol{q}}^{J'}\rangle$ and apply the Löwdin orthogonalization,

$$|\tilde{\zeta}_{\boldsymbol{q}}^J\rangle = \sum_{J'} |\zeta_{\boldsymbol{q}}^{J'}\rangle(S_{\boldsymbol{q}}^{-1/2})_{J'J}. \tag{23}$$

The set $\left\{|\tilde{\zeta}_{\boldsymbol{q}}^J\rangle\right\}$ is both smooth in $\boldsymbol{q}$ and orthonormal. Now, localized excitonic states can be constructed through a Fourier transform,

$$|\Xi_\mu^J\rangle = \frac{1}{\sqrt{N}} \sum_{\boldsymbol{q}} e^{-i\boldsymbol{q}\cdot\boldsymbol{r}_\mu} |\tilde{\zeta}_{\boldsymbol{q}}^J\rangle. \tag{24}$$

In particular, for one isolated excitonic band in 1D, we can use $|\Phi_{i_0,\nu,\uparrow}^{a_0,\nu,\uparrow}\rangle$ as the target function, where i_0 and a_0 are Wannier functions from the valence and conduction bands. The diabatization is then a simple two-step procedure,

$$|\tilde{\xi}_q\rangle \equiv |\xi_q\rangle \frac{\langle\xi_q|\Phi_{i_0,\nu,\uparrow}^{a_0,\nu,\uparrow}\rangle}{\left|\langle\xi_q|\Phi_{i_0,\nu,\uparrow}^{a_0,\nu,\uparrow}\rangle\right|}, \tag{25}$$

$$|\Xi_\mu\rangle \equiv \frac{1}{\sqrt{N}} \sum_q e^{-iqR_\mu} |\tilde{\xi}_q\rangle. \tag{26}$$

We will show below that, perhaps unsurprisingly, Eqs. (25) and (26) work very well if the HF single-particle band energies do not overlap, and there is a significant energy separation between HOMO and HOMO − 1 (and between LUMO and LUMO + 1). In such a case, the single-particle Bloch bands will not cross, and the gauge fixed in Eq. (25) should be reasonable. Indeed, this separation is obeyed for the one-dimensional model in Sec. II A.

More generally, one should be able to construct MLWFs when single-particle bands cross[52,63,64] and generate reasonable target functions. Note that crossing single-particle bands and crossing excitonic bands are very different phenomena. After all, there is no impediment to single-particle bands crossing away from the Fermi level, whereas excitonic bands will always try to avoid each other (as a result of diagonalization). That being said, in higher dimensions (i.e., two and three dimensional systems), we expect that degenerate or avoided crossings of single-particle and/or excitonic bands can be common. In such a case, Eqs. (25) and (26) should work well if one can isolate a meaningful basis of target (localized) Wannier excitations (just like constructing localized single-particle WFs through "subspace selection via projection" in the entangled single-particle band case[63,64]). However, generating the optimal target functions may not always be obvious.

2. Method #2

With this background, let us now offer two new and more general diabatization schemes. Method #2 follows the spirit of Pipek-Mezey localization. For this scheme, we generate localized diabatic states by optimizing the expectation value of the following target function:

$$f_{PM}(U) = \sum_{\mu B} \sum_{\nu,i,a} \left(\langle\Xi_\mu^B|P^{ia\nu}|\Xi_\mu^B\rangle\right)^2, \tag{27}$$

where

$$P^{ia\nu} = |\Phi_{i,\nu}^{a,\nu}\rangle\langle\Phi_{i,\nu}^{a,\nu}|. \tag{28}$$

Recall the definition of U in Eq. (20). For this paper, for the sake of convenience, we will focus on the case of just a single excitonic band (so we may ignore the label B).

In practice the function f_{PM} can be maximized through successive pairwise unitary transforms[54] (also called Jacobi sweeps),

$$\begin{pmatrix}\tilde{\Xi}_\mu & \tilde{\Xi}_{\mu'}\end{pmatrix} = \begin{pmatrix}\Xi_\mu & \Xi_{\mu'}\end{pmatrix} \begin{pmatrix}\cos\gamma & -\sin\gamma e^{-i\theta} \\ \sin\gamma e^{i\theta} & \cos\gamma\end{pmatrix}. \tag{29}$$

Starting with $U = I$, we apply 2×2 unitary transforms on pairs of states $|\Xi\rangle$. For each transform, γ and θ are chosen so that f_{PM} is maximized. For each 2×2 transform,

$$\begin{aligned} L(\ldots,\tilde{\Xi}_\mu,\ldots,\tilde{\Xi}_{\mu'},\ldots) &= L(\ldots,\Xi_\mu,\ldots,\Xi_{\mu'},\ldots) \\ &+ A_{\mu\mu'} + (A_{\mu\mu'}^2 + B_{\mu\mu'}^2)^{1/2}\cos 4(\gamma-\alpha), \end{aligned} \tag{30}$$

with

$$\begin{aligned} A_{\mu\mu'} &= \sum_{i,a,\nu} \frac{1}{4}(e^{i\theta}P_{\mu\mu'}^{ia\nu} + e^{-i\theta}P_{\mu'\mu}^{ia\nu})^2 - \frac{1}{4}\left(P_{\mu\mu}^{ia\nu} - P_{\mu'\mu'}^{ia\nu}\right)^2, \\ B_{\mu\mu'} &= \sum_{i,a,\nu} \frac{1}{2}\left(e^{i\theta}P_{\mu\mu'}^{ia\nu} + e^{-i\theta}P_{\mu'\mu}^{ia\nu}\right)\cdot(P_{\mu\mu}^{ia\nu} - P_{\mu'\mu'}^{ia\nu}), \\ \cos 4\alpha &= -A_{\mu\mu'}/(A_{\mu\mu'}^2 + B_{\mu\mu'}^2)^{1/2}, \\ \sin 4\alpha &= B_{\mu\mu'}/(A_{\mu\mu'}^2 + B_{\mu\mu'}^2)^{1/2}. \end{aligned} \tag{31}$$

The optimal θ is found by brute force on a grid so as to maximize $A_{\mu\mu'} + (A_{\mu\mu'}^2 + B_{\mu\mu'}^2)^{1/2}$. For a total of N $\{|\xi_q\rangle\}$ states, a sweep contains $N(N-1)/2$ transforms. $|\Xi\rangle$ usually converges in a few sweeps. Note that the Jacobi sweeps in Eqs. (29)–(31) are slightly different than those suggested long ago by Edmiston and Ruedenberg[54] because we must treat complex, unitary 2×2 transformation (rather than real 2×2 rotations).

3. Method #3

Our third and final method is the generalization of Boys localized diabatization for excitons in solids. For our purposes, since excitons are electrically neutral, a maximization criterion based on charge centers is not natural. Instead, restricting ourselves to excited state wavefunctions constructed with CIS or TD-DFT or BSE, we will maximize the separation between the electron/hole (attachment/detachment[56]) densities in the same spirit as BoysOV localized diabatization.

Thus, following Eq. (11), if $|\Xi_\mu^B\rangle = \sum_{qI} |\xi_q^I\rangle U_{qI,\mu B} = \sum_{i\tilde{a}} s_{i\tilde{a}}^{(\mu B)} |\Phi_i^{\tilde{a}}\rangle$, periodic BoysOV localized diabatization maximizes the following target function:

$$s^{(I)}_{\tilde{i}\tilde{a}} = \sum_J t^{(J)}_{\tilde{i}\tilde{a}} U_{JI}, \tag{32}$$

$$\begin{aligned} f^{diab}_{BoysOV-periodic}(U) &= \sum_{\mu B}\sum_d \left(\sum_{\tilde{i}\tilde{j}\tilde{a}} (s^{(\mu B)}_{\tilde{i}\tilde{a}})^* \langle \phi_{\tilde{j}} | X^{(d)} | \phi_{\tilde{i}} \rangle s^{(\mu B)}_{\tilde{j}\tilde{a}} \right)^2 \\ &+ \sum_{\mu B}\sum_d \left(\sum_{\tilde{i}\tilde{a}\tilde{b}} (s^{(\mu B)}_{\tilde{i}\tilde{a}})^* \langle \phi_{\tilde{a}} | X^{(d)} | \phi_{\tilde{b}} \rangle s^{(\mu B)}_{\tilde{i}\tilde{b}} \right)^2 \\ &= \sum_{\mu B}\sum_d \left[\mathrm{Tr}\left((\underline{X}^{(d)}_{occ})^T \underline{S}^{(\mu B)} (\underline{S}^{(\mu B)})^\dagger \right) \right]^2 \\ &+ \sum_{\mu B}\sum_d \left[\mathrm{Tr}\left((\underline{X}^{(d)}_{vir})^T (\underline{S}^{(\mu B)})^\dagger \underline{S}^{(\mu B)} \right) \right]^2 . \end{aligned}$$

Here, $\underline{S}^{(\mu B)}$, $\underline{X}^{(d)}_{occ}$, and $\underline{X}^{(d)}_{vir}$ are matrices, $(\underline{S}^{(\mu B)})_{\tilde{i}\tilde{a}} = s^{(\mu B)}_{\tilde{i}\tilde{a}}$, $(\underline{X}^{(d)}_{occ})_{\tilde{i}\tilde{j}} = \langle \phi_{\tilde{i}} | X^{(d)} | \phi_{\tilde{j}} \rangle$, and $(\underline{X}^{(d)}_{vir})_{\tilde{a}\tilde{b}} = \langle \phi_{\tilde{a}} | X^{(d)} | \phi_{\tilde{b}} \rangle$. In practice, the diabatization can be accomplished with Jacobi sweeps. If there is only one excitonic band to diabatize, one can simply follow Eqs. (29)–(31) assuming that one replaces $A_{\mu\mu'}$ and $B_{\mu\mu'}$ with

$$\begin{aligned} A_{\mu\mu'} &= \sum_d \frac{1}{4}\left(e^{i\theta}\bar{\underline{X}}^{(d)}_{\mu\mu'} + e^{-i\theta}\bar{\underline{X}}^{(d)}_{\mu'\mu} \right)^2 - \frac{1}{4}\left(\bar{\underline{X}}^{(d)}_{\mu\mu} - \bar{\underline{X}}^{(d)}_{\mu'\mu'} \right)^2 \\ &+ \sum_d \frac{1}{4}\left(e^{i\theta}\tilde{\underline{X}}^{(d)}_{\mu\mu'} + e^{-i\theta}\tilde{\underline{X}}^{(d)}_{\mu'\mu} \right)^2 - \frac{1}{4}\left(\tilde{\underline{X}}^{(d)}_{\mu\mu} - \tilde{\underline{X}}^{(d)}_{\mu'\mu'} \right)^2, \\ B_{\mu\mu'} &= \sum_d \frac{1}{2}\left(e^{i\theta}\bar{\underline{X}}^{(d)}_{\mu\mu'} + e^{-i\theta}\bar{\underline{X}}^{(d)}_{\mu'\mu} \right)\left(\bar{\underline{X}}^{(d)}_{\mu\mu} - \bar{\underline{X}}^{(d)}_{\mu'\mu'} \right) \\ &+ \sum_d \frac{1}{2}\left(e^{i\theta}\tilde{\underline{X}}^{(d)}_{\mu\mu'} + e^{-i\theta}\tilde{\underline{X}}^{(d)}_{\mu'\mu} \right)\left(\tilde{\underline{X}}^{(d)}_{\mu\mu} - \tilde{\underline{X}}^{(d)}_{\mu'\mu'} \right), \end{aligned} \tag{33}$$

where $\bar{\underline{X}}^{(d)}_{\mu\mu'} \equiv \mathrm{Tr}\left((\underline{X}^{(d)}_{occ})^T \underline{S}^{(\mu)} (\underline{S}^{(\mu)})^\dagger \right)$ and $\tilde{\underline{X}}^{(d)}_{\mu\mu'} \equiv \mathrm{Tr}\left((\underline{X}^{(d)}_{vir})^T (\underline{S}^{(\mu)})^\dagger \underline{S}^{(\mu)} \right)$.

D. Nuances

In the end, no matter how we construct the ADT matrix U, the diabatic Hamiltonian is

$$H_{diab} = U^\dagger \Lambda U, \tag{34}$$

where $\Lambda \equiv \mathrm{diag}(\omega_{\xi_{q1}}, \ldots, \omega_{\xi_{qN}})$ and the diabatic couplings emerge as the off-diagonal elements of H_{diab}. At this point, we must point out one unusual nuance. Namely, for the case of only a single excitonic band, in order to obtain the diabatic Hamiltonian, one does not always need to go through the complicated diabatization above. In particular, because of translational symmetry, if we restrict ourselves to the case of a single excitonic band, we know that the adiabatic-to-diabatic transformation must be more or less equivalent to a Fourier transform. For instance, consider the first approach above and a single excitonic band [Eqs. (25) and (26)]. Note that a direct Fourier transform of the exciton band will suffice to generate diabatic couplings. To prove that such an approach will be effective, note that fixing the gauge of the Bloch excitations before rotating Bloch states into localized wave functions (with transformation $U^{(0)}_{q\mu} = \exp(-iqR_\mu)$) is equivalent to substituting $U^{(0)} \to DU^{(0)}$ where $D = \mathrm{diag}(e^{i\theta_1}, \ldots, e^{i\theta_n})$. Now, observe that $(DU^{(0)})^\dagger \Lambda (DU^{(0)}) = (U^{(0)})^\dagger \Lambda U^{(0)}$, because Λ is diagonal, so that the choice of gauge for the Bloch excitations has no effect on H_{diab}.

Despite this curious finding, one should not over-interpret this curious result. First, note that, for all the matrix elements of all other operators, for example the dipole moment, we absolutely will require the phase matrix D and the full diabatization. Second, we emphasize that, without carefully choosing the gauge, the states generated by a Fourier transform do not have any chemical or physical meaning. Third and finally, if we must diabatize multiple excitonic bands, it is clear that a simple Fourier transform will never suffice.

For all of these reasons, it is essential that we generate meaningful ADT matrices: simple Fourier transforms are not enough.

III. RESULTS

A. Excitonic band

We have run CIS calculations [Eq. (15)] with 2 filled and 2 empty bands. We will now present the results of excited-state diabatization calculations. To begin our discussion, the nature of the CIS excited states was interrogated with

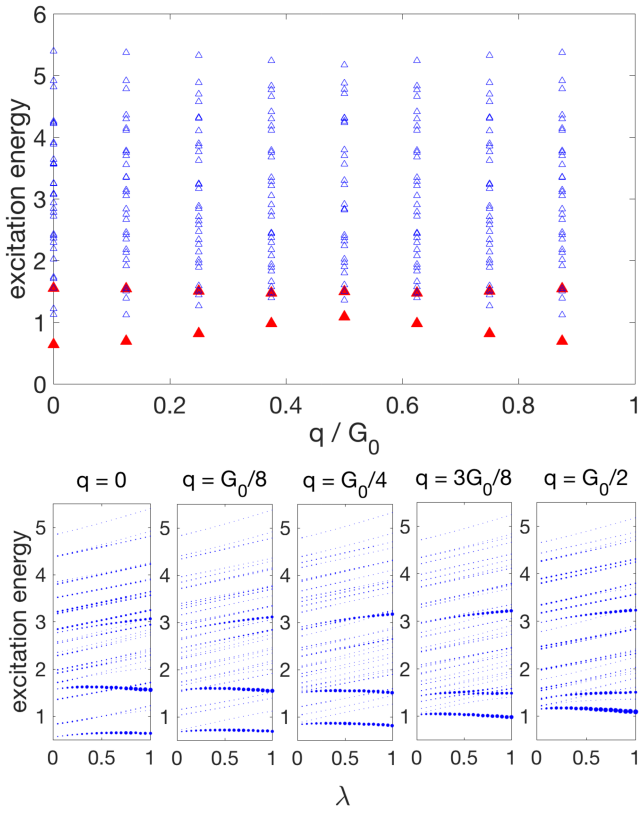

FIG. 3. (Upper) Excitation energies from a CIS calculation as a function of the excitonic momentum q with $\lambda = 1$, $N = 8$. Here, N is the number of unit cells (i.e., k points). The potential and the single-particle band structure have been plotted in Fig. 2. G_0 is the unit reciprocal lattice vector. Only triplet states are plotted. The red dots are identified as exciton bands with significant locality; (lower) the excitation energies as a function of λ which is defined in Eq. (12). The size of the dots is proportional to the localization criterion [Eq. (19)], which confirms our identification of excitonic states above.

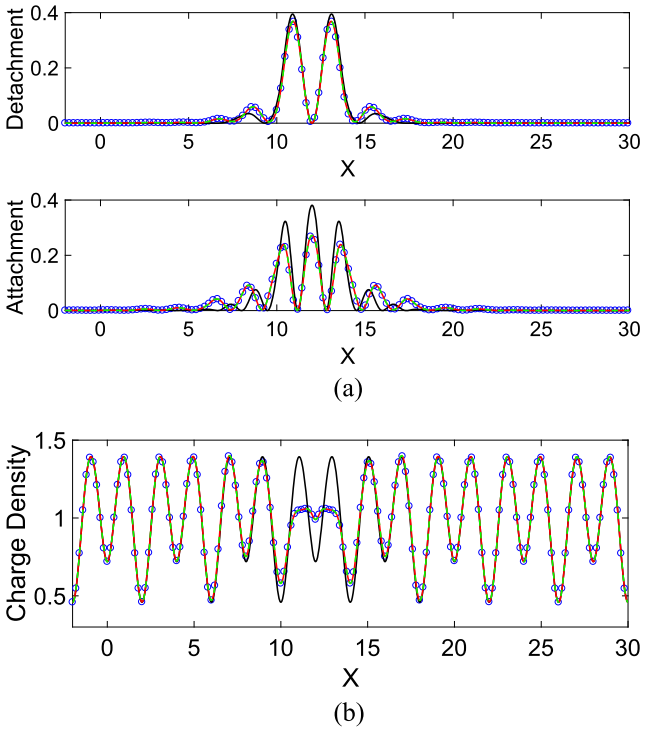

FIG. 4. Here we set λ = 1 and study the Frenkel limit for localized excitons. The length of one unit cell is 4. MLWFs are used for methods #1 and #2. (a) Detachment and attachment densities are plotted for the localized Wannier excitation $|\Phi_{i_0,\nu}^{a_0,\nu}\rangle$ (which is the target function for the method #1) in black. We plot the same attachment/detachment densities for diabatic states from methods #1, #2, and #3 in blue, red, and green. Note that all diabatic states agree with each other and mostly with the target function as well. (b) Charge density of a diabatized excitonic state (which is localized to the fourth unit cell) as a function of position x. Methods #1, #2, and #3 are plotted in blue, red, and green, respectively. In black, we plot the ground state charge density.

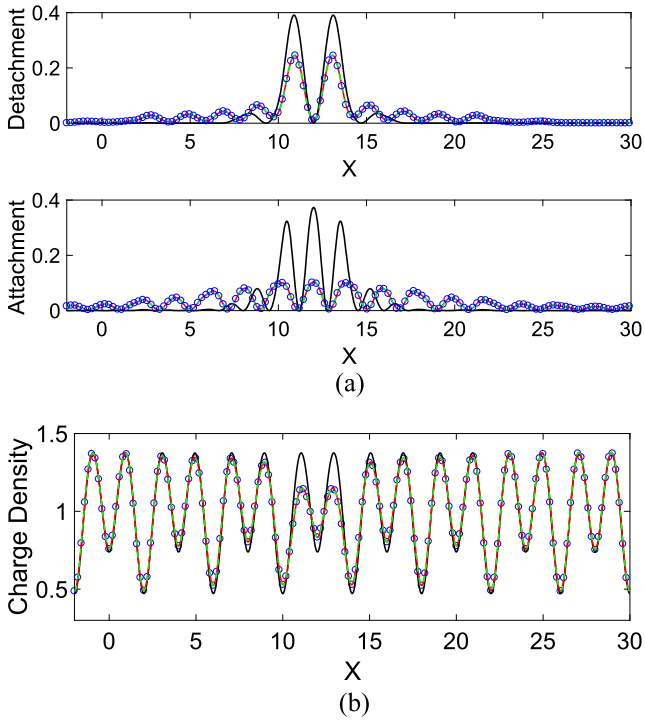

FIG. 5. Same calculation as Fig. 4 except that λ = 0.06. Excitons in this case are near the Wannier-Mott limit. Note that we can still generate localized excitonic states even in this limit; however, the resulting states have lost much of their resemblance to the original target functions.

both the scaling approach and locality criterion [Eq. (19)]. Results are shown in Fig. 3. For a system with very weak effective $e-e$ interactions (small λ), our results show no excited states with significant locality; this conclusion can be justified by noting that, in the bottom part of Fig. 3, the blue dots become weaker and weaker at small λ. This finding is consistent with the notion that excitons will have a radius larger than the lattice size when the $e-e$ interaction is strongly screened, resulting in Wannier-Mott excitons.

In our model, the lowest excitation band is always the exciton band, which should not be surprising. While most excitation energies grow with an increasing effective $e-e$ interaction, excitonic energies are less sensitive and can even decrease. A crude argument is that $e-e$ interactions can generally be viewed as increasing energy gaps by forcibly separating electrons. At the same time, however, excitons are electron-hole pairs with a negative binding energy whose absolute value must grow with an increasing $e-h$ interaction which grows with λ. According to our calculations, these two effects seem to compensate for each other in the case of our one-dimensional excitonic states.

B. Diabatization

Given the results in Fig. 3, we will now diabatize the lowest (excitonic) band.

1. Analyzing the wavefunction

In Figs. 4 and 5, we plot the charge densities of the resulting diabatized state. As expected, for the case of large λ, these charge densities are effectively the same as the charge density of the ground state except in one unit cell; for the case of small λ, differences are spread out over a few adjacent cells. Thus, the resulting diabatic states can be interpreted as either single localized Frenkel or Wannier-Mott excitons, respectively.

In Figs. 4 and 5, we also plot the attachment/detachment densities of all relevant diabatic states versus the target function in method #1 (which is a localized Wannier excitation). The differences are small in the Frenkel limit: this result might have been expected because Frenkel excitons are completely

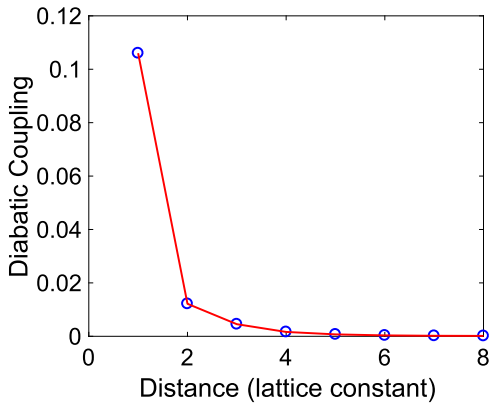

FIG. 6. Diabatic coupling vs. site distance in units of the lattice constant. Results are based on our method #2 with λ = 1, N = 16. Note the quick decay; for many purposes, only nearest neighbor couplings are necessary.

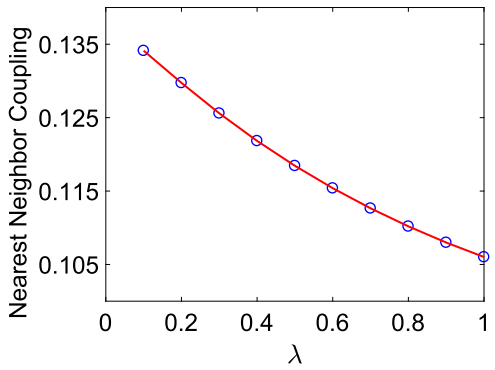

FIG. 7. Nearest neighbor coupling vs. λ. Results are based on our method #2 with $N = 16$. In systems where the Coulomb interaction is strongly screened (small λ which is the Wannier-Mott limit), excitons are more delocalized and have stronger couplings with their neighbors.

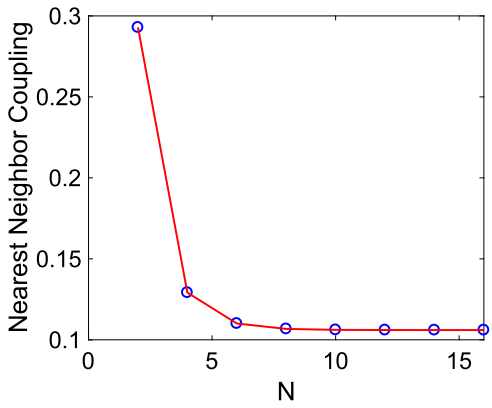

FIG. 8. Nearest neighbor coupling vs. N (the number of k points or, equivalently, unit cells). λ is set to be 1. Data from the method #2. Note that, for a converged calculation, one requires at least $N = 4$ unit cells. The relative error between $N = 8$ and 16 is less than 1%. These electronic couplings are essential for modeling excitation states coupled to nuclear motion in the limit of large electron-phonon coupling.

localized and can be expressed as a superposition of localized Wannier excitations. Furthermore, in our 1D semiconductor model, the valence band and the conduction band are well-distinguished and do not overlap with other single-particle, so that the character of the lowest CIS excitation band is obvious.

2. Electronic couplings

We now turn to the diabatic, electronic couplings between diabatized states. In Fig. 6, we plot these couplings as a function of site distance for large λ. The nearest-neighbor couplings are much larger than couplings between excitonic diabats far apart, as would be expected. The decay with site distance appears to be exponential and the results would seem to justify keeping only nearest neighbor coupling in tight-binding Hamiltonians. Note that, if we include phonon motion, these diabatic couplings are the key ingredients for modeling incoherent energy transfer in the limit of large electron-phonon couplings: they are useful both to generate model Hamiltonians and to express Fermi's Golden Rule (FGR) (i.e., Marcus) rates.

Next, in Fig. 7, we plot the nearest neighbor coupling as a function of λ. In systems where the effective $e - e$ interaction is strongly screened (small λ), excitons on neighboring sites can have significant overlap which leads to a relatively large coupling.

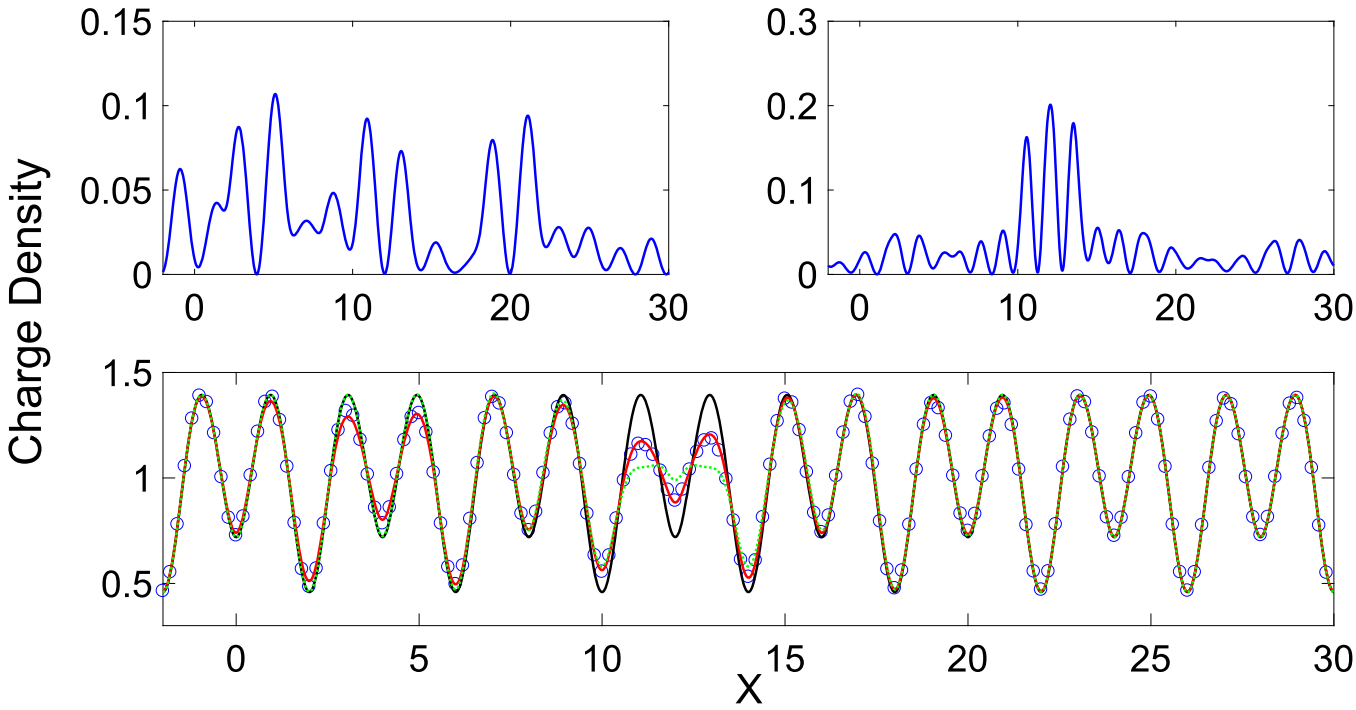

FIG. 9. Here we set λ = 1 and compare method #3 (green) with methods #1 and #2 (blue and red). The latter two approaches rely on localized single-particle WFs and, for the present example, the valence and conduction WFs are plotted in the upper left and right panels, respectively. Note that these WF's are far less localized than MLWFs (e.g., look carefully around X = 5). The resulting diabatic states from methods #1 and #2 are clearly delocalized and suboptimal. By contrast, method #3 is insensitive to the choice of single-particle WFs, which is a relative advantage. In black, we plot the ground state charge density.

In Fig. 8, we explore excitonic interactions as a function of the total number of non-trivial unit cells in our system (i.e., the number of k points). We plot the corresponding nearest neighbor diabatic coupling. We find that we require about 8 cells in order for the error to be less than 1%. Interestingly, the diabatic coupling appears to converge more quickly than the HOMO-LUMO energy gap, which requires 12 or more unit cells before convergence to within 1%.

IV. DISCUSSION

Before concluding, we feel it necessary to highlight the sensitivity of diabatization methods #1 and #2 to the nature of single-particle WFs. In Fig. 9, we plot the charge density that is predicted by all of the different diabatization methods. In this case, we invoke a poor choice of WFs; namely, here we build WF's without a consistent gauge for each Bloch state. As a result, the WF for the valence band is very poorly localized. Note that, with this suboptimal choice of single-particle WFs, methods #1 and #2 give awkward, delocalized diabatic states. By contrast, method #3 is unaffected. This difference highlights one relative advantage of Boys localization. At the same time, we note that, if MLWFs are used, all the three methods give almost identical results in our model. See Fig. 9.

V. CONCLUSION

We have proposed three methods to generate localized, diabatic excitonic states. These methods will certainly work in the Frenkel regime; they should also be effective in the moderately delocalized Wannier-Mott regime. Our model system has been a one-dimensional molecular crystal, but all of these approaches can be applied in any dimension:

- The first algorithm is a simple projection scheme based on the most naive algorithm to generate one-particle Wannier functions; this algorithm will work best when the conduction and valence bands are well-separated from all other bands.
- The second algorithm mimics the Pipek-Mezey orbital localization scheme and maximizes a target function with respect to the expectation value of Wannier projection operators.
- The third algorithm generalizes Boys localized diabatization to excitons in periodic systems through (i) introducing a set of "cyclically permuted" position operators and (ii) focusing on the attachment/detachment densities [Eq. (10)] instead of the total charge density. This method is restricted to CIS/TD-DFT/BSE excited states, where attachments and detachment can be uniquely defined.

All of the methods above have performed equally well in our model system above, but the latter two algorithms should perform better in higher dimensions with more complicated systems and crossing bands.

In the end, localized diabatic states are essential for modeling nonadiabatic processes in systems with large electron-phonon couplings: they are useful both to generate model Hamiltonians and to express FGR (i.e., Marcus) rates. Thus, when combined with high-level excited state calculations, the methods above should be very useful in modeling both singlet and triplet energy transfer in molecular crystals.

ACKNOWLEDGMENTS

This material is based upon work supported by the (U.S.) Air Force Office of Scientific Research (USAFOSR) PECASE Award under AFOSR Grant No. FA9950-13-1-0157. J.E.S. gratefully acknowledges support from the Stanford PULSE Institute, a John Simon Guggenheim Memorial Fellowship, and a David and Lucile Packard Fellowship.

[1] D. Beljonne, C. Curutchet, G. D. Scholes, and R. J. Silbey, J. Phys. Chem. B **113**, 6583 (2009).
[2] G. D. Mahan, *Many-Particle Physics* (Springer Science & Business Media, 2013).
[3] W. Hanke and L. J. Sham, Phys. Rev. Lett. **43**, 387 (1979).
[4] S. Albrecht, L. Reining, R. Del Sole, and G. Onida, Phys. Rev. Lett. **80**, 4510 (1998).
[5] L. X. Benedict, E. L. Shirley, and R. B. Bohn, Phys. Rev. Lett. **80**, 4514 (1998).
[6] M. Rohlfing and S. G. Louie, Phys. Rev. Lett. **81**, 2312 (1998).
[7] M. Rohlfing and S. G. Louie, Phys. Rev. B **62**, 4927 (2000).
[8] M. Gatti and F. Sottile, Phys. Rev. B **88**, 155113 (2013).
[9] P. Cudazzo, L. Sponza, C. Giorgetti, L. Reining, F. Sottile, and M. Gatti, Phys. Rev. Lett. **116**, 066803 (2016).
[10] S. Sharifzadeh, P. Darancet, L. Kronik, and J. B. Neaton, J. Phys. Chem. Lett. **4**, 2197 (2013).
[11] E. Runge and E. K. U. Gross, Phys. Rev. Lett. **52**, 997 (1984).
[12] E. Gross and W. Kohn, Adv. Quantum Chem. **21**, 255 (1990).
[13] F. Furche and R. Ahlrichs, J. Chem. Phys. **117**, 7433 (2002).
[14] S. Refaely-Abramson, M. Jain, S. Sharifzadeh, J. B. Neaton, and L. Kronik, Phys. Rev. B **92**, 081204 (2015).
[15] A. Marini, R. Del Sole, and A. Rubio, Phys. Rev. Lett. **91**, 256402 (2003).
[16] L. Reining, V. Olevano, A. Rubio, and G. Onida, Phys. Rev. Lett. **88**, 066404 (2002).
[17] C.-C. Lee, H. C. Hsueh, and W. Ku, Phys. Rev. B **82**, 081106 (2010).
[18] L. Kronik and J. B. Neaton, Annu. Rev. Phys. Chem. **67**, 587 (2016).
[19] T. Holstein, Ann. Phys. **8**, 325 (1959).
[20] Y.-C. Cheng and R. J. Silbey, J. Chem. Phys. **128**, 114713 (2008).
[21] A. Nitzan, *Chemical Dynamics in Condensed Phases: Relaxation, Transfer and Reactions in Condensed Molecular Systems* (Oxford University Press, 2006).
[22] M. Baer, Chem. Phys. Lett. **35**, 112 (1975).
[23] M. Baer, Mol. Phys. **40**, 1011 (1980).
[24] R. G. Sadygov and D. R. Yarkony, J. Chem. Phys. **109**, 20 (1998).
[25] D. R. Yarkony, J. Phys. Chem. A **102**, 8073 (1998).
[26] X. Zhu and D. R. Yarkony, J. Chem. Phys. **140**, 024112 (2014).
[27] X. Zhu and D. R. Yarkony, J. Chem. Phys. **144**, 044104 (2016).
[28] K. Ruedenberg and G. J. Atchity, J. Chem. Phys. **99**, 3799 (1993).
[29] G. J. Atchity and K. Ruedenberg, Theor. Chem. Acc.: Theory Comput. Model. (Theor. Chim. Acta) **97**, 47 (1997).
[30] H. Nakamura and D. G. Truhlar, J. Chem. Phys. **115**, 10353 (2001).
[31] H. Nakamura and D. G. Truhlar, J. Chem. Phys. **117**, 5576 (2002).
[32] H. Nakamura and D. G. Truhlar, J. Chem. Phys. **118**, 6816 (2003).
[33] R. J. Cave and M. D. Newton, Chem. Phys. Lett. **249**, 15 (1996).
[34] R. J. Cave and M. D. Newton, J. Chem. Phys. **106**, 9213 (1997).
[35] A. A. Voityuk and N. Rösch, J. Chem. Phys. **117**, 5607 (2002).
[36] A. A. Voityuk, J. Chem. Phys. **140**, 244117 (2014).
[37] H.-C. Chen, Z.-Q. You, and C.-P. Hsu, J. Chem. Phys. **129**, 084708 (2008).
[38] C.-P. Hsu, Z.-Q. You, and H.-C. Chen, J. Phys. Chem. C **112**, 1204 (2008).
[39] C.-P. Hsu, Acc. Chem. Res. **42**, 509 (2009).
[40] J. E. Subotnik, S. Yeganeh, R. J. Cave, and M. A. Ratner, J. Chem. Phys. **129**, 244101 (2008).
[41] J. E. Subotnik, R. J. Cave, R. P. Steele, and N. Shenvi, J. Chem. Phys. **130**, 234102 (2009).
[42] J. E. Subotnik, E. C. Alguire, Q. Ou, B. R. Landry, and S. Fatehi, Acc. Chem. Res. **48**, 1340 (2015).
[43] T. Pacher, L. Cederbaum, and H. Köppel, J. Chem. Phys. **89**, 7367 (1988).

[44]T. Pacher, L. Cederbaum, and H. Köppel, *Advances in Chemical Physics* (John Wiley & Sons, Inc., 1993), Vol. 84, p. 293.
[45]P. H. Dederichs, S. Blügel, R. Zeller, and H. Akai, Phys. Rev. Lett. **53**, 2512 (1984).
[46]T. A. Wesolowski and A. Warshel, J. Phys. Chem. **97**, 8050 (1993).
[47]M. H. M. Olsson, G. Hong, and A. Warshel, J. Am. Chem. Soc. **125**, 5025 (2003).
[48]J. Neugebauer, M. J. Louwerse, E. J. Baerends, and T. A. Wesolowski, J. Chem. Phys. **122**, 094115 (2005).
[49]M. Pavanello and J. Neugebauer, J. Chem. Phys. **135**, 234103 (2011).
[50]J. Foster and S. Boys, Rev. Mod. Phys. **32**, 300 (1960).
[51]D. A. Kleier, T. A. Halgren, J. H. Hall, and W. N. Lipscomb, J. Chem. Phys. **61**, 3905 (1974).
[52]N. Marzari and D. Vanderbilt, Phys. Rev. B **56**, 12847 (1997).
[53]E. Blount, *Solid State Physics* (Elsevier, 1962), Vol. 13, p. 305.
[54]C. Edmiston and K. Ruedenberg, Rev. Mod. Phys. **35**, 457 (1963).
[55]J. E. Subotnik, J. Vura-Weis, A. J. Sodt, and M. A. Ratner, J. Phys. Chem. A **114**, 8665 (2010).
[56]M. Head-Gordon, A. M. Grana, D. Maurice, and C. A. White, J. Phys. Chem. **99**, 14261 (1995).
[57]E. Ö. Jónsson, S. Lehtola, M. J. Puska, and H. Jonsson, J. Chem. Theory Comput. **13**, 460 (2017).
[58]A one-dimensional integral of the Fourier transform of $1/r$, $\int \mathrm{d}q(4\pi/q^2)$, diverges near zero, making the average energy per particle scales with N.
[59]A. Gold and A. Ghazali, Phys. Rev. B **41**, 7626 (1990).
[60]T. Giamarchi, *Quantum Physics in One Dimension* (Oxford University Press, 2004).
[61]S. Hirata and M. Head-Gordon, Chem. Phys. Lett. **314**, 291 (1999).
[62]S. Bernadotte, F. Evers, and C. R. Jacob, J. Phys. Chem. C **117**, 1863 (2013).
[63]N. Marzari, A. A. Mostofi, J. R. Yates, I. Souza, and D. Vanderbilt, Rev. Mod. Phys. **84**, 1419 (2012).
[64]I. Souza, N. Marzari, and D. Vanderbilt, Phys. Rev. B **65**, 035109 (2001).